Scientia Iranica B (2023) 30(1), 39–51

Sharif University of Technology
Scientia Iranica
Transactions B: Mechanical Engineering
http://scientiairanica.sharif.edu

Experimental and numerical investigation of flow behaviors of some selected food supplements in modeled intestine

S.E. Ibitoye[a,*], I.K. Adegun[a], O.A. Olayemi[b], P.O. Omoniyi[a], and O.O. Alabi[a]

a. *Department of Mechanical Engineering, University of Ilorin, PMB 1515, Ilorin, Nigeria.*
b. *Department of Aeronautics and Astronautics, Faculty of Engineering and Technology, Kwara State University, Malete, Kwara State, Nigeria.*

Received 14 March 2022; received in revised form 9 June 2022; accepted 15 August 2022

KEYWORDS
Digestive system;
Fluid flow;
Pressure;
Modelled intestine;
Small intestine;
Velocity.

Abstract. This study presents the flow of Hibiscus Sabdariffa Roselle (Sobo), Soymilk (Soya), and Pap (Ogi) through a modeled intestine. Experimental and Computational Fluid Dynamics (CFD) techniques were employed, while Autodesk Inventor 2020 version was used to draw the 3D computational model of the human intestine. ANSYS Fluent 16.0 was utilized as a CFD solver. Deformed boundary walls of the Navier-stokes equations of fluid flow were used for modeling. The results showed that fluid velocity, pressure, density, and viscosity significantly affected the flow behavior of nutrients in the intestinal walls. The density and viscosity of the investigated fluids ranged between 800–1024 kg/m^3 and 0.316–1.095 Pas, respectively, while the maximum and minimum viscosities were observed with Ogi and Sobo, respectively. The highest drop in the velocity along the whole length of the intestinal model ranged between 0.8 and 1.5 m, which corresponded to the pulsating section of the model. The maximum and minimum Reynolds numbers were recorded with Sobo and Ogi samples, respectively. To ensure effective flow and avoid complications when taking food supplements, a flow velocity of 0.005 m/s is recommended. The presence of villi in the intestinal wall augmented heat transfer.

1. Introduction

Global attention to the computational simulation of fluid flow, heat transfer components, and modeling of human intestine is growing so as to deep current understanding of its complex behavior for healthy living [1–3]. The utilization of Computational Fluid Dynamics (CFD) as an affordable, crucial, and accurate technique to comprehend the process and transport the human intestine activities is becoming reliable and popular [4–9]. This technique facilitates the analysis, treatment, and management of gastrointestinal-related diseases and the development of new food supplements for human growth and well-being. Given the preceding, researchers have renewed interest in the study of fluid flow of steady-state, hydrodynamics, laminar, non-Newtonian, viscous fluids in a pulsating medium due to its widespread biomedical and engineering applications (chemical systems and digestive systems of living organisms) [10–13].

In the human body, food digestion begins in the mouth. This is where food is masticated and moisturized by the saliva amylase; it goes down into

*. *Corresponding author. Tel.: +2347036113237*
E-mail address: ibitoye.s@unilorin.edu.ng (S.E. Ibitoye)

doi: 10.24200/sci.2022.60130.6613

the stomach through the gullet by peristaltic movements [14]. Peristalsis is contraction in a wave-like form of the intestinal wall, forcing the fluid forward like a peristaltic pump [5,15–19]. According to Imam et al. [20], the process of peristalsis begins in the esophagus when food is swallowed and taken to the small intestine, where it blends, mixes, and moves Chyme back and forth for nutrients to be delivered and absorbed into the bloodstream through small intestine walls.

The movement of fluid within the small intestine can be categorized into three patterns: peristalsis, pendular, and segmentation movements [21–24]. In pendular movement, Chyme does not propel along the intestinal tract. It discreetly blends and slices the food for proper digestion. On the other hand, segmentation and peristalsis propel Chyme through the small intestine via sinusoidal muscular shrinkage. The frequency and force of intestinal contractions function as slow waves and action potentials in peristalsis [25,26]. Peristalsis pushes Chyme via the intestine in about 180–360 s with an average velocity of 1.67×10^{-4} m/s [27,28].

The small intestine is an extremely multilayered void organ situated in the top portion of the alimentary path [18,29]. When humans take liquid and solid food, liquid foods usually move and get down to the stomach before solid food, and this food leaves the stomach at different times. However, it takes solid food and molten Chyme equal to energy density of about 21/2 h to permeate via the small intestine for body utilization [30,31]. Having adequate knowledge of fluid flow in the intestine is essential for good *in vitro-in vivo* relationships for evaluating the effect of food preparation on nutrient absorption. Tharakan et al. [32] observed that the movement and delivery of nutrients to the intestine depended on the rate of controlling step of absorption. Based on the obtained reports, fluid dynamics affect the absorption and transmission of food minerals and vitamins to the intestinal wall; therefore, it affects the delivery and assimilation profiles as a function of fluid properties. This results from the convective blending of contents in the intestine and discharges from the body with diffusion via food mixture.

Digestion of food can be grouped into chemical and mechanical digestion. Chemical digestion accounted for the breakdown of lipids, proteins, and carbohydrates into a smaller unit that the cell films can absorb through catabolic reaction. On the other hand, mechanical digestion is the moving process that enhances the blending of food and displacement via the gastrointestinal tract. The lifeless behaviors of biological fluids can be categorized into the non-Newtonian or Newtonian fluids [6,33,34]. Newtonian fluids are fluids with constant viscosity, and the viscosity is independent of the pressure applied to the fluid. Conversely, non-Newtonians have no constant viscosity; when enough force is applied to this fluid, the viscosity changes. Most biological fluids present viscous and elastic features via synchronized repository and delivery of mechanical energy [35,36].

A comprehensive review of the numerical extrapolation of pharmacokinetic characteristics and in-vitro structures of the intestine to model oral drug disposition could be found in [12,13]. Marrero et al. [37] conducted a state-of-the-art review on different technologies, resources, and structures used to imitate the intestine functionality and control pertinent physiological factors. Critical scrutiny of the current challenges, necessities, and drawbacks of the micro-atmosphere imitation of in-vitro microfluidic system models was also conducted.

It is essential to comprehend the food breakdown and delivery of controlled foods in the intestine to develop foods with health benefits, human growth, and development. Therefore, this study seeks to carry out an experimental and numerical investigation into some parameters that affect the delivery of some selected food supplements (nutrients) to the intestinal walls. This covers the flow parameters such as velocity, Reynolds number pressure, and fluid physical properties by simulating intestinal flow profiles. This research advances available knowledge on the utilization of Soymilk, *Hibiscus Sabdariffa Roselle*, and Pap as food supplements using modeling and simulation techniques. This study found biomedical engineering applications in the development of food delivery tools for life sciences and medical applications. Moreover, our results facilitate the analysis, treatment, control, and management of gastrointestinal-related diseases and the development of new food supplements for human growth and well-being.

2. Methodology

2.1. Materials

The materials used for this study are Soymilk, *Hibiscus Sabdariffa Roselle*, and Pap. These materials were sourced from an open market in Ogbomoso, Oyo State, Nigeria.

2.2. Methods

2.2.1. Computational tools and model

A 3-D computational model of the human intestine was drawn using Autodesk Invertor 2020 version. The stable flow field generated in the modeled intestine due to the motion of shrinkage waves was simulated. Deformed boundary walls of the Navier-stokes equations of the fluid flow were used for the model, and ANSYS Fluent 16.0 was employed as the CFD solver. The model and mesh profile of the intestine are shown in Figure 1.

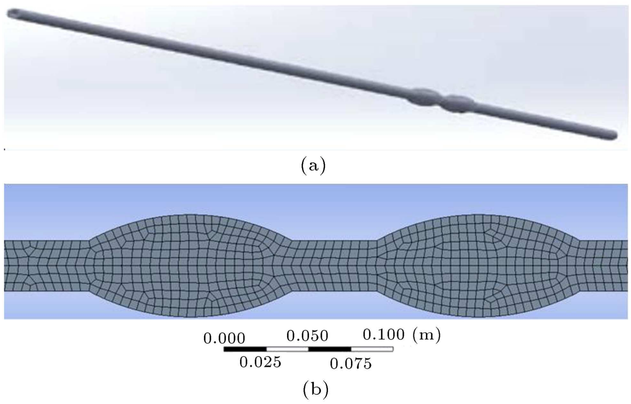

Figure 1. (a) Intestinal model and (b) mesh profile.

2.2.2. Preparation of Soymilk (Soya), Pap (Ogi), and Hibiscus Sabdariffa Roselle (Sobo) samples

The collected dry beans of Soya were sorted to separate unwanted materials, after which they were soaked in water for a minimum of 3 h. The rehydrated beans were then wet ground to form the desired slurry of the final product, which has the protein content. About 50 ml of the resulting slurry was boiled in a stainless steel port to improve its taste and flavor and to sterilize the product. The slurry was continuously heated at or near the boiling point for 15–20 minutes. The boiled slurry was filtered to remove the insoluble residues. The resulting solution was collected and kept in glass bottles for further analysis.

The Sobo was handpicked to remove dirt. About 200 g of the raw sample was cleaned in a sterile 5-liter beaker after being lightly washed and boiled with 2 liters of water for ten minutes. The excerpts were received instantaneously and filtered using a neat, germ-free muslin cloth. The filtrates were received and stored in pre-sanitized bottles for further analysis.

The cereals of the Ogi were collected and sorted from unwanted materials, after which they were soaked in water at room temperature for 3–5 days. The water used for the soaking process was changed every 24 h and replaced with a fresh one until a frothing foam was formed on top of the setup with an alcoholic smell. After foam with alcoholic smell formation, the cereals were adequately washed on the wet ground to form a slurry. The slurry was filtered with a neat, uninfected muslin cloth, and the filtrates were collected. About 10 ml of water was boiled in a stainless steel pot to the boiling point, after which 30 ml of the filtrate was added and heated continuously for 10 minutes to form the pap. The pap was collected and kept in glass bottles for further analysis.

2.2.3. Physical properties of prepared samples

The density of the prepared samples was estimated by measuring the mass of a known volume of each sample. The density was calculated using Eq. (1) [38]. The viscosity of the prepared samples was determined using the Stokes' law (falling sphere method), as described by Yusuf et al. [39]. Steel spheres of known density and diameter were made to fall freely via a straight transparent glass tube of 1.5 m height. The transparent glass tube was filled with prepared samples, and the time taken for the sphere to fall between the heights of 0.2–1 m in the transparent glass was measured using a digital stopwatch. The velocity of the falling sphere was calculated using Eq. (2) [38], while the viscosity was determined using Eq. (3) [38]. The experiment was repeated using four different steel spheres and the average was reported.

$$\rho = \frac{m}{V}, \tag{1}$$

$$v_s = \frac{d}{t}, \tag{2}$$

$$\mu = \frac{2r_s^2(\rho_s - \rho)g}{9v}, \tag{3}$$

where ρ is the sample density, m mass of the samples, V volume of the samples, d falling distance by the sphere, t time, μ viscosity of the prepared samples, r_s, ρ_s, and v_s are the radius, density, and velocity of the sphere, respectively, and g the acceleration due to gravity.

2.2.4. Governing equations

The model is governed by Navier-stokes and continuity equations according to the following assumptions:

i. The flow is laminar natural convection;
ii. The fluid flow is steady-state hydrodynamic and incompressible;
iii. The inlet temperature is 303 K;
iv. The velocity profile is entirely developed in the model;
v. Gravitational effect is neglected;
vi. The no-slip boundary condition at the walls is considered;
vii. Constant heat flux thermal boundary condition is applied.

2.3. Continuity equation

The continuity equation is presented in Eq. (4) [23,40]:

$$\frac{\partial \bar{U}}{\partial \bar{R}} + \frac{\bar{U}}{\bar{R}} + \frac{\partial \bar{W}}{\partial \bar{W}} = 0. \tag{4}$$

2.3.1. Momentum equation

The momentum equations are given in Eqs. (5) and (13) [23,40].

Radial direction:

$$\rho\left(\frac{\partial}{\partial\bar{t}}+\bar{U}\frac{\partial}{\partial\bar{R}}+\bar{W}\frac{\partial}{\partial\bar{Z}}\right)\bar{U}=-\frac{\partial\bar{P}}{\partial\bar{R}}$$
$$+\frac{1}{R}\frac{\partial}{\partial\bar{R}}\left(\bar{R}_{\tau\bar{R}\bar{R}}\right)-\frac{1}{R}\left(\tau_{\bar{Z}\bar{Z}}\right). \quad (5)$$

Azimuthal direction:

$$\rho\left(\frac{\partial}{\partial\bar{t}}+\bar{U}\frac{\partial}{\partial\bar{R}}+\bar{W}\frac{\partial}{\partial\bar{Z}}\right)\bar{W}=-\frac{\partial\bar{P}}{\partial\bar{Z}}$$
$$+\frac{1}{R}\frac{\partial}{\partial\bar{R}}\left(\bar{R}_{\tau\bar{R}\bar{Z}}\right)+\frac{\partial}{\partial\bar{Z}}\left(\bar{R}\tau_{\bar{Z}\bar{Z}}\right). \quad (6)$$

2.3.2. Energy equation

The energy equation is presented in Eqs. 7–13 [23,40]:

$$\rho C_p\left(\frac{\partial}{\partial\bar{t}}+\bar{U}\frac{\partial}{\partial\bar{R}}+\bar{W}\frac{\partial}{\partial\bar{Z}}\right)\bar{T}=\tau\bar{R}\bar{R}\frac{\partial\bar{U}}{\partial\bar{R}}$$
$$+\tau\bar{R}\bar{Z}\frac{\partial\bar{W}}{\partial\bar{R}}+\tau\bar{Z}\bar{Z}\frac{\partial\bar{U}}{\partial\bar{Z}}+\tau\bar{R}\bar{Z}\frac{\partial\bar{W}}{\partial\bar{Z}}$$
$$+K\left(\frac{\partial^2\bar{T}}{\partial\bar{R}^2}+\frac{1}{\bar{R}}\frac{\partial\bar{T}}{\partial\bar{R}}+\frac{\partial^2\bar{T}}{\partial\bar{Z}^2}\right), \quad (7)$$

$$\bar{\tau}=\left[\mu_\infty+(\mu_O+\mu_\infty)\left(1-\Gamma\left|\bar{\dot{\gamma}}\right|^{-1}\right)\bar{\dot{\gamma}}\right], \quad (8)$$

$$\left|\bar{\dot{\gamma}}\right|=\sqrt{\frac{1}{2}\sum_i\sum_j\bar{\dot{\gamma}}_{ij}\bar{\dot{\gamma}}_{ji}}=\sqrt{\frac{1}{2}\prod}, \quad (9)$$

$$\prod=\left(gradV+(gradV)^T\right)^2, \quad (10)$$

$$\tau\bar{R}\bar{R}=2\mu_O\left(1+\Gamma\left|\bar{\dot{\gamma}}\right|\right)\frac{\partial\bar{U}}{\partial\bar{R}}, \quad (11)$$

$$\tau\bar{R}\bar{Z}=\mu_O\left(1+\Gamma\left|\bar{\dot{\gamma}}\right|\right)\left(\frac{\partial\bar{U}}{\partial\bar{Z}}+\frac{\partial\bar{W}}{\partial\bar{R}}\right), \quad (12)$$

$$\tau\bar{Z}\bar{Z}=2\mu_O\left(1+\Gamma\left|\bar{\dot{\gamma}}\right|\right)\left(\frac{\partial\bar{W}}{\partial\bar{Z}}\right). \quad (13)$$

2.3.3. Computational procedure and numerical algorithm

The geometry of the investigated esophagus was drawn by ANSYS design modeler. Thereafter, a mesh dependence test was conducted, and the optimum mesh (Figure 1) was used for all the conducted simulations. The properties of various fluids including Chyme, Ogi, Soya, and Sobo were inputted appropriately. The no-slip boundary condition was imposed on the solid boundaries of the model. Then, the equations governing the flow dynamics and heat transport in the investigated model were then solved using ANSYS (Fluent 16.0 version) software, whose functioning relies on the finite volume method. Given that the flow is

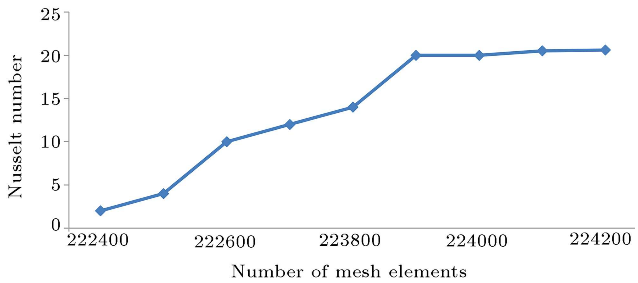

Figure 2. Mesh convergence graph.

Table 1. Physical properties of prepared fluid samples at 20°C.

Fluids	Density (kg/m^3)	Viscosity (Pas)
Chyme	1000	1.0
Ogi	1024	1.095
Soya	920	0.95
Sobo	800	0.316

incompressible, a pressure-based solver was employed and the inlet velocity was set at 0.005 m/s. The convergence criterion was set as 1.0e-07. The mesh convergence graph is shown in Figure 2.

3. Results and discussion

3.1. Physical properties of the prepared samples

Table 1 shows the physical properties of the samples prepared at 20°C. The viscosity of the samples varied between 0.316–1.095 Pas, while their density varied between 800–1024 kg/m^3. Sobo and Ogi had the lowest and highest densities, respectively. The maximum and minimum viscosities were observed for Ogi and Sobo, respectively. It was found that the higher the viscosity, the smaller the inner friction and the lower the resistance of the fluid to flow [39]. However, this property is dependent on temperature. Analysis results for the physical properties illustrate that Sobo had the least resistance to flow, followed by Soya and Chyme, while Ogi exhibited the highest resistance to flow.

3.2. Velocity

Figures 3 and 4 show the velocity contours of the non-Newtonian fluid flow across the entire length and the pulsating part in rhythmical porous media of the intestinal model. There was a no-slip boundary condition, and velocity was equal to zero at the walls. Fluid velocity was higher around the inlet and outlet, but lower at the pulsating area. This was due to the enlarged surface area occasioned by the expansion of the pulsating part mimicking the non-uniform nature of the real human intestine; these affect the number of nutrients delivered to the intestinal walls. The larger surface area made possible by expansion through the

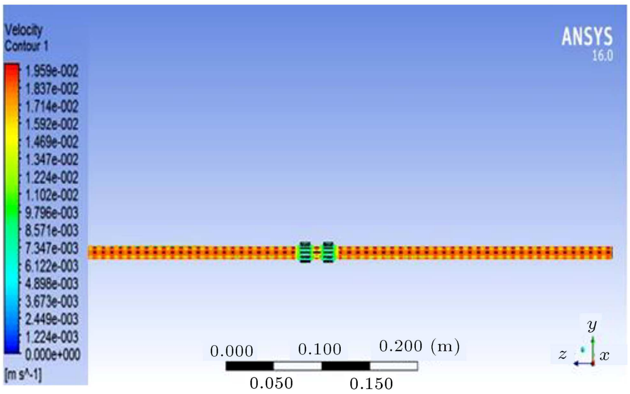

Figure 3. Velocity profile across the span of the modeled intestine.

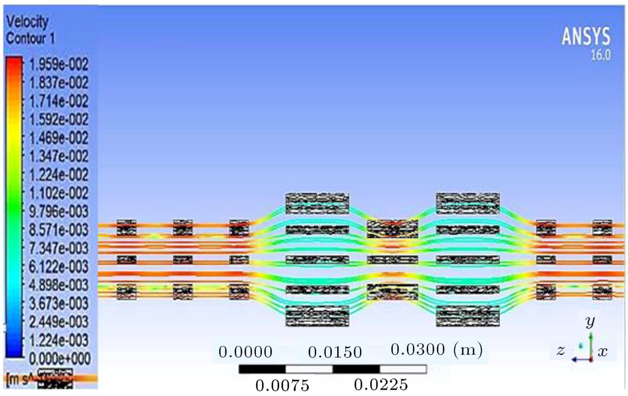

Figure 4. Velocity profile for the pulsating part of the modeled intestine.

peristaltic movement of the walls leads to a lower flow rate; hence, more nutrients will be delivered to the intestinal walls. This expansion was due to villi in the intestine, affecting the amount of heat transferred. Therefore, a larger surface area due to the expansion implies better heat transfer. The higher the velocity, the lower the flow rate, while the greater the amount of heat that will be transferred. The presence of villi in the intestine points to the wave-like nature of the internal walls. It improves the absorption characteristics of the intestinal walls as well as heat transfer properties [23].

The velocity profiles along the intestinal model cross-section and velocity streamlines are presented in Figures 5–9. The figures reveal the velocity profile via the cross duct sections at 0.8, 1.1, 1.5, and 2.3 m of the model, respectively. It could be observed that the velocity of the fluid is gradually reduced as it flows along with the intestine model. A decline in velocity was observed at some point and later increased as the fluid flowed. Reduction in the velocity was more pronounced between 0.8 and 1.5 m, coinciding with the pulsating section of the model. The drop in the velocity resulted from the expansion in this region, as revealed by the profile. This variation aligns with the

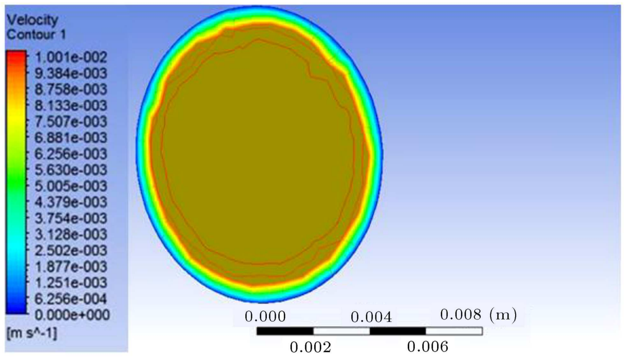

Figure 5. Velocity profile along the cross duct section at 0.8 m of the modeled intestine.

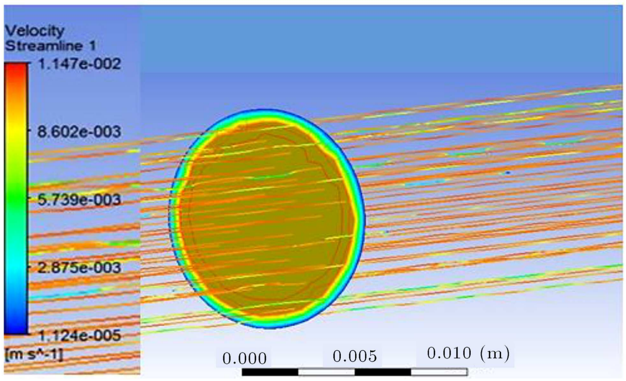

Figure 6. Velocity streamline along the cross duct section at 0.8 m of the modeled intestine.

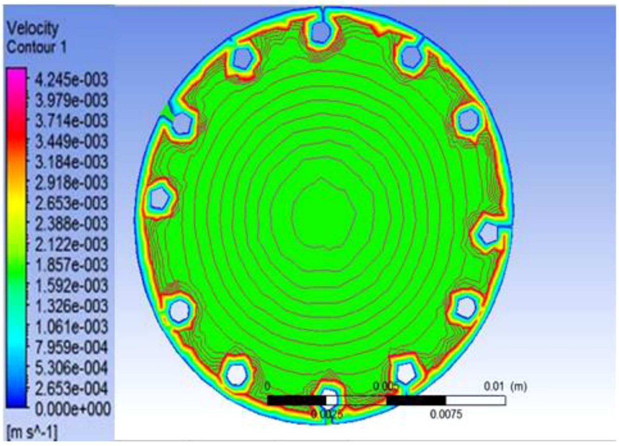

Figure 7. Velocity profile along the cross duct section at 1.1 m of the modeled intestine.

scientific fact that the larger the cross-sectional area, the lower the fluid flow velocity in a duct. The velocity variation enhances fluid absorption by intestinal walls and intensifies the peristaltic motion of the fluid in the intestine.

Figures 10–13 show the fluid flow at different inlet velocities along with the axial positions. There was a propulsive movement of the intestine, pushing the fluid towards the aboral end of the intestine. This

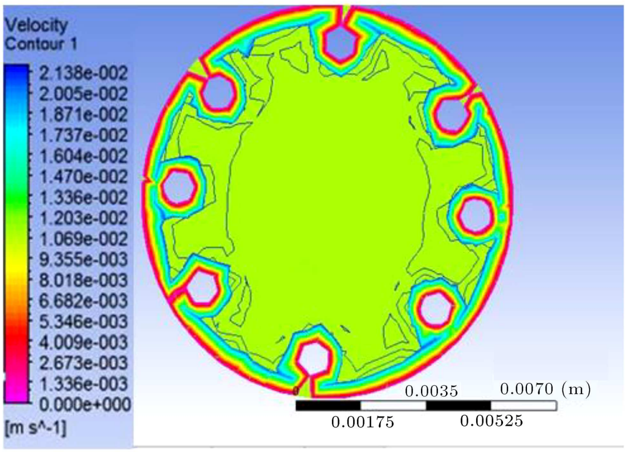

Figure 8. Velocity profile along the cross duct section at 1.5 m of the modeled intestine.

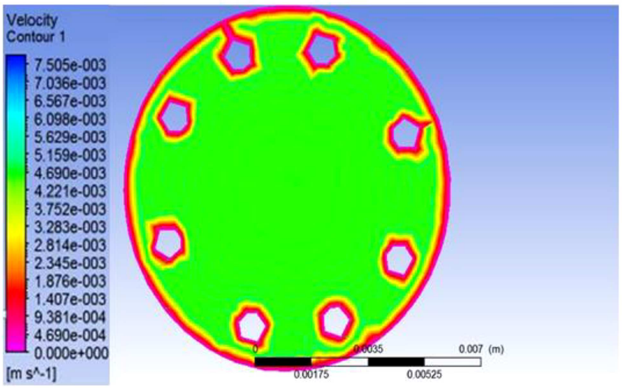

Figure 9. Velocity profile along the cross duct section at 2.3 m of the modeled intestine.

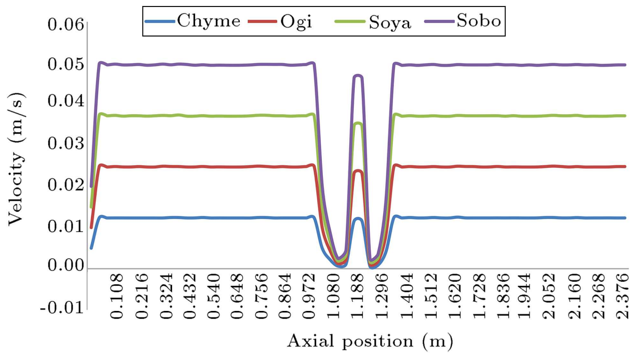

Figure 10. Flow velocity with axial position along the centerline of the domain at an inlet velocity of 0.005 m/s.

was observed for all the fluid samples considered. It can be observed that the velocity increased given characteristics of propulsive wave-like propagation to the point of 1.1 m at different inlet velocities, and it remained constant up to the pulsating portion of the intestinal model, where the velocity suddenly falls and later rises to the end. In addition, peristaltic movement of an intestine of wave-like propagation was relaxed as velocity increased at all inlet velocities of the

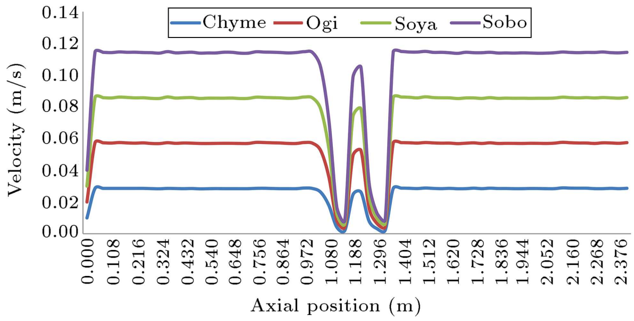

Figure 11. Flow velocity with axial position along the centerline of the domain at an inlet velocity of 0.01 m/s.

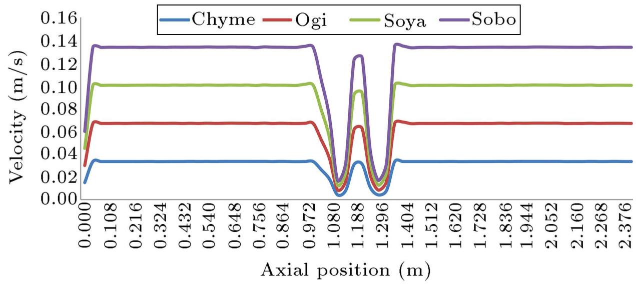

Figure 12. Flow velocity with axial position along the centerline of the domain at an inlet velocity of 0.015 m/s.

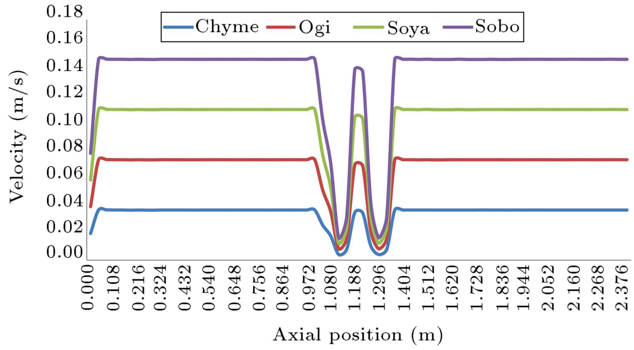

Figure 13. Flow velocity with axial position along the centerline of the domain at an inlet velocity of 0.02 m/s.

fluids. Contraction of peristaltic movement occurred when the velocity dropped in the pulsating parts of the intestinal model and later proceeded with the relaxation of peristaltic movement to the end. It was observed that relaxations always come before and after the contraction.

In Figure 14, all the fluids comply with the relaxation and contraction of peristaltic movements of an intestine, and all have the same velocity variation along with the axial positions. There are optimum and maximum velocities at the center due to the effect of friction in villi.

3.3. Pressure

Figures 15 and 16 present the pressure profiles across the length and pulsating part of the intestinal model,

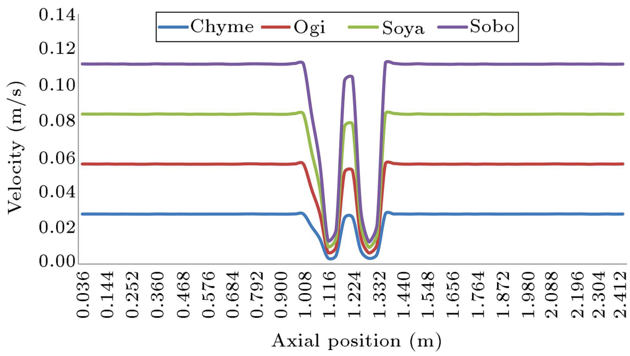

Figure 14. Average velocity with the axial position for different fluids.

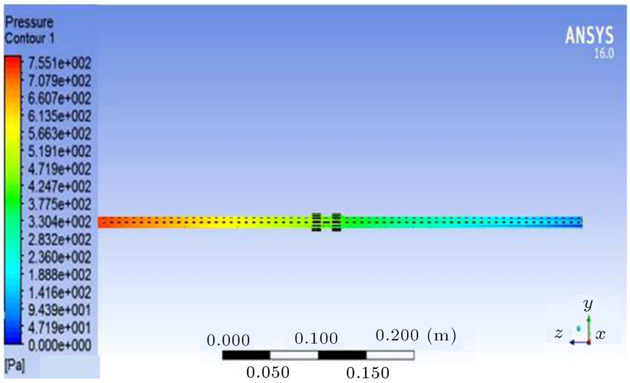

Figure 15. Pressure profile through the length of the modeled intestine.

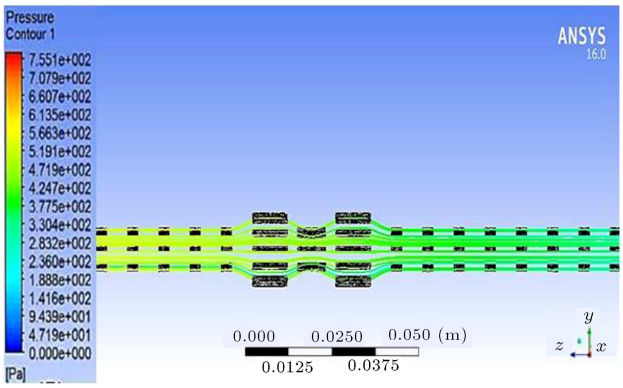

Figure 16. Pressure profile for the pulsating portion of the modeled intestine.

respectively. It can be observed that the flow is laminar and the pressure contour is fully developed. Figures 17–20 display variation in flow pressure with the axial position through the centerline of the domain at different inlet velocities. The figures reveal that pressure decreases from the inlet to the outlet along with the axial positions for all inlet velocities. From the position 1.1–1.5 m, there was an increase in the surface area of the pulsating part of the model, resulting in a change in the height of the folds. These are observed in the human intestine which enhance

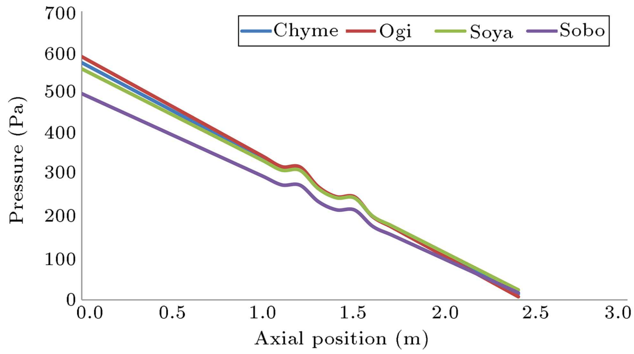

Figure 17. Flow pressure with axial position via the centerline of the domain at an inlet velocity of 0.005 m/s.

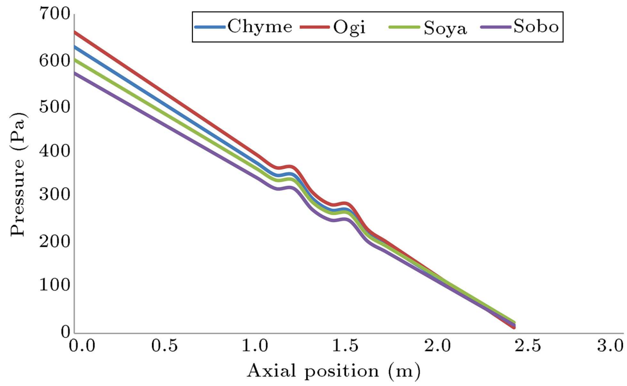

Figure 18. Flow pressure with axial position via the centerline of the domain at an inlet velocity of 0.01 m/s.

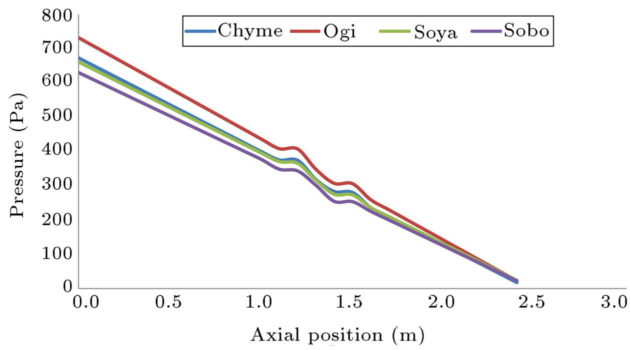

Figure 19. Flow pressure with axial position via the centerline of the domain at an inlet velocity of 0.015 m/s.

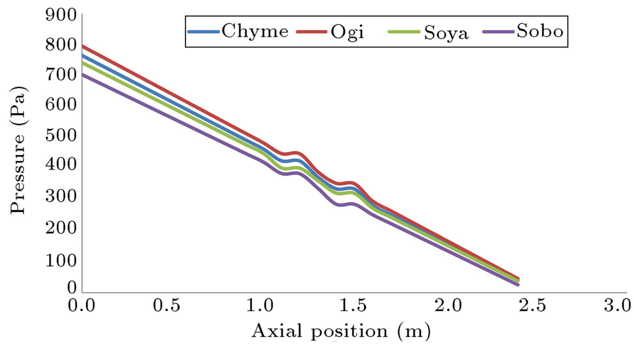

Figure 20. Flow pressure with axial position via the centerline of the domain at an inlet velocity of 0.02 m/s.

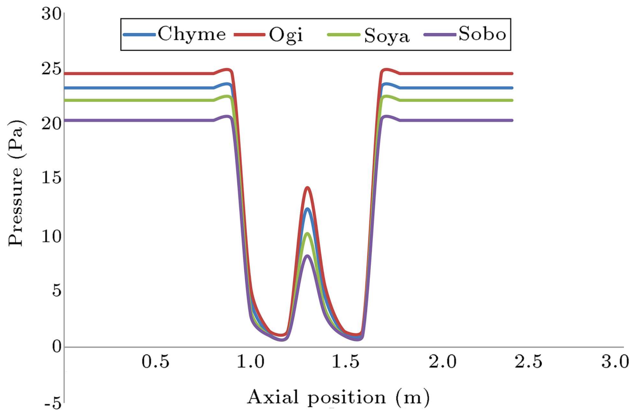

Figure 21. Change in pressure with the axial position for different fluids at an inlet velocity of 0.005 m/s.

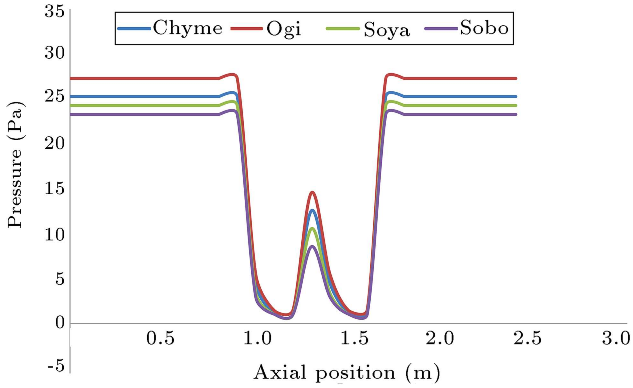

Figure 22. Change in pressure with the axial position for different fluids at an inlet velocity of 0.01 m/s.

nutrient delivery. The fold passively increased the absorptive surface area of the intestine. It was also observed that the viscosity of each fluid has a significant impact on the intestine due to the peristaltic force and pressure of the fluid motion. High viscosity gives rise to high pressure on the intestine walls and a lower fluid flow rate. High pressure enhances intestinal wall expansion with better nutrient delivery due to a larger surface area by the exerted pressures. Therefore, expansion due to pressure and villi augmented heat transfer.

Figures 21–24 show the plots of pressure variation with the axial position for different fluid samples. The fluid inlet pressure varied between 20.31–24.52 Pa. At about 1 m of the intestine, the pressure dropped suddenly due to the fluctuating flow. The implication is that the velocity of flowing fluid will be low, which will improve the number of nutrients delivered to the intestinal walls. Similar observations were made for all the inlet velocities at 1.3 m. The sudden drop along the axial position was due to the fold of the intestine, and it later increased at the exit. Among all the fluids considered, Ogi exerted highest pressure, while Sobo sample exerted the least; this phenomenon results from the difference in the physical properties

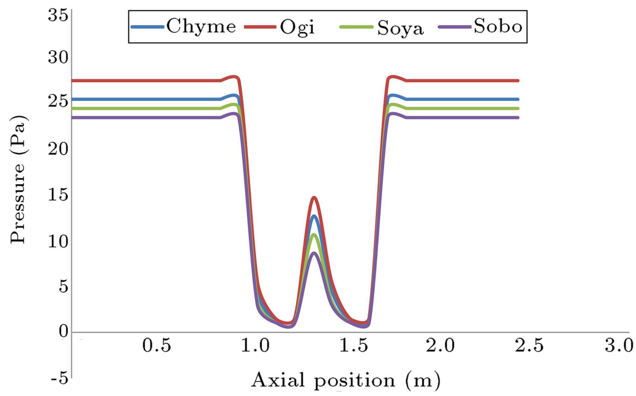

Figure 23. Change in pressure with the axial position for different fluids at an inlet velocity of 0.015 m/s.

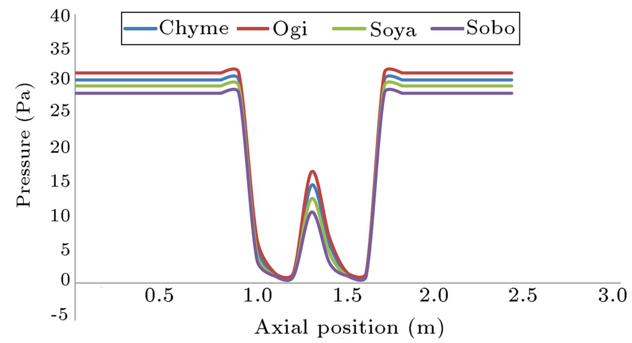

Figure 24. Change in pressure with the axial position for different fluids at an inlet velocity of 0.02 m/s.

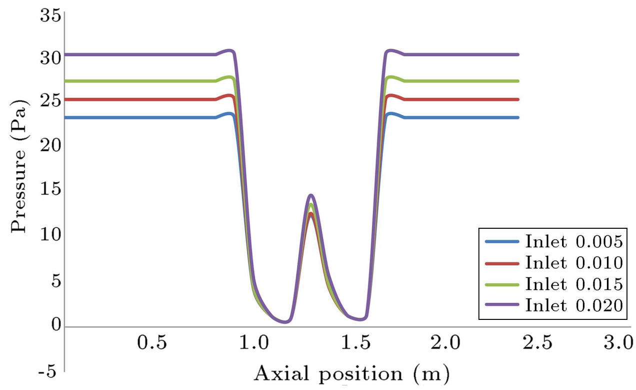

Figure 25. Change in pressure with the axial position for Chyme.

of the fluid (Table 1). It was observed that Ogi had the highest pressure followed by Chyme, Soya, and Sobo at every inlet velocity. It can also be observed from Figures 25–28 that inlet velocity changes with pressure and fluid flow for all fluids considered. To ensure effective fluid flow and avoid complications when consuming these food supplements, especially for someone under medication, a flow velocity of 0.005 m/s is recommended. This is within the range predicted for Chyme by Ibitoye et al. [41]. Furthermore, Sobo could function as an antioxidant because of its high-pressure drop [1,29,42,43].

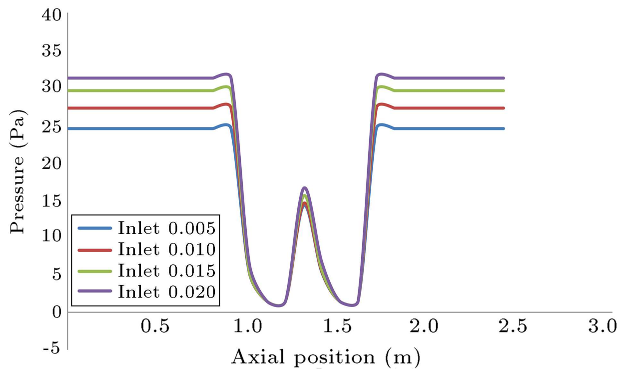

Figure 26. Change in pressure with the axial position for Ogi.

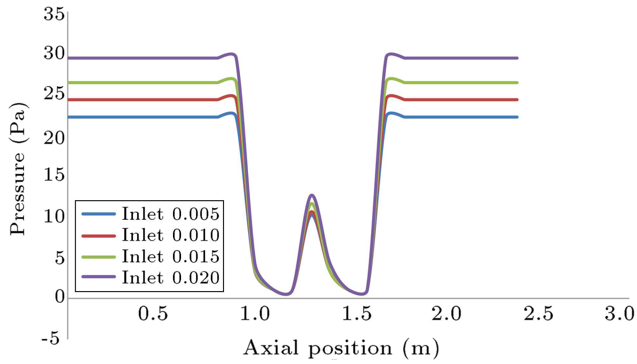

Figure 27. Change in pressure with the axial position for Soya.

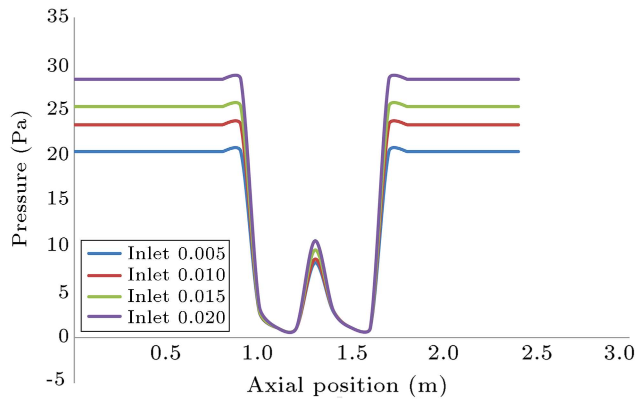

Figure 28. Change in pressure with the axial position for Sobo.

3.4. Reynolds number

Figures 29–32 show the variation of average velocity with Reynolds number along the length of the intestinal model at different inlet velocities. It was observed that the Reynolds number increased with an increase in velocity for all the fluids. The highest Reynolds number was observed for the Sobo sample due to its low density and viscosity, compared with other samples (Table 1). The highest Reynolds number, after Sobo, corresponds to Soya, Chime, and Ogi, in order, for all the inlet velocities used for the investigation. This implies that under the same condition, the fluid delivery rate to the

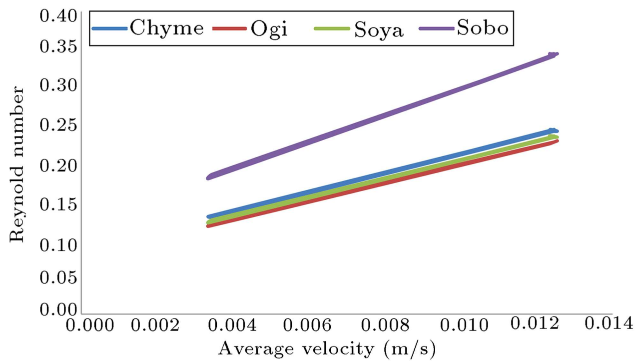

Figure 29. Average velocity with Reynolds number via the length of the modeled intestine at 0.005 m/s inlet velocity.

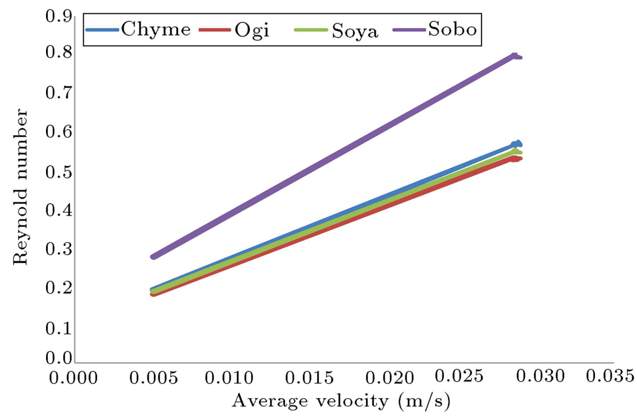

Figure 30. Average velocity with Reynolds number via the length of the modeled intestine at 0.01 m/s inlet velocity.

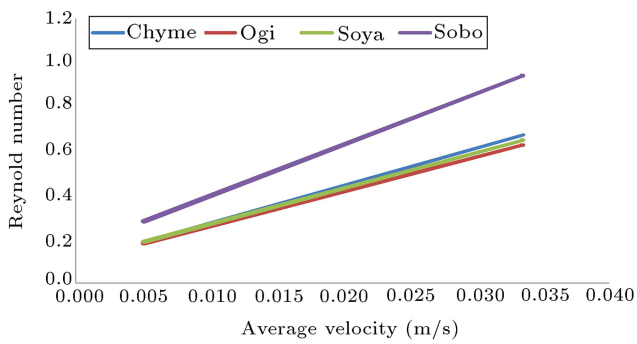

Figure 31. Average velocity with Reynolds number via the length of the modeled intestine at 0.015 m/s inlet velocity.

intestinal walls differs and Sobo is the best based on this study. The result of this study is in line with the observation of Ismail [44], who reported that the inlet velocity increases steadily up to a certain point before it suddenly falls in the pulsating part of the tube and then, rises to the end of the flow.

4. Validation of results

To underscore the robustness and accuracy of the

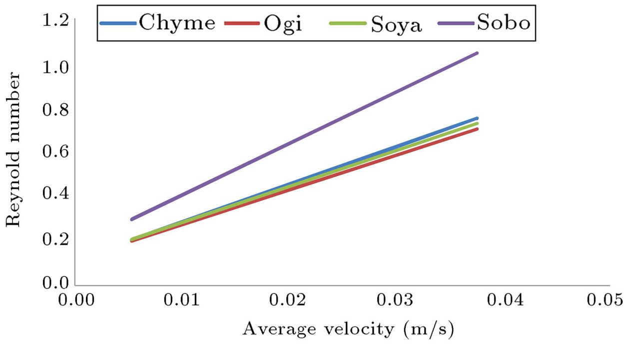

Figure 32. Average velocity with Reynolds number via the length of the modeled intestine at 0.02 m/s inlet velocity.

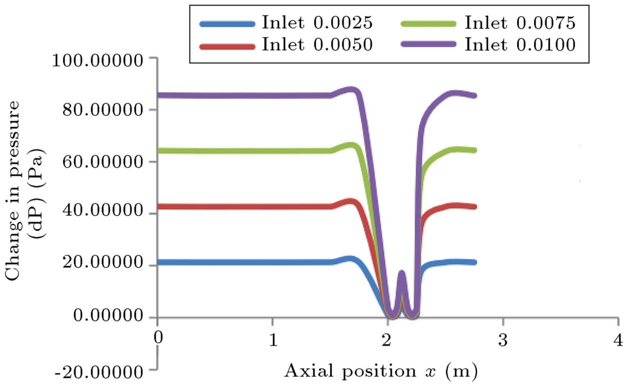

Figure 33. Variation of pressure with inlet velocities and axial position [1].

current investigation, the trend of the plots from the present investigation (see Figures 21–28) was compared with that found by Adegun et al. [1] (Figure 33). In addition, the trends of both studies were found to be of good fit. The optimum velocity of 0.005 m/s recommended in this study for effective flow when taking food supplements, especially for someone under medication, is within the range of 0.0025–0.01 m/s submitted by Adegun et al. [1].

5. Conclusions

Experimental and numerical investigation of non-Newtonian viscous fluids in a rhythmical porous medium was carried out, and ranges of inlet velocities and pressures were examined. The density and viscosity of the investigated fluids were in the range of 800–1024 kg/m^3 and 0.316–1.095 Pas, respectively, while the maximum and the minimum viscosity were observed in the case of Ogi and Sobo, respectively. The fluid inlet pressure varied between 20.31–24.52 Pa. A sudden drop in pressure of about 1 m along the intestine led to the delivery of more nutrients to the intestinal walls. The highest drop in velocity along the whole length of the intestinal model was noticed between 0.8 and 1.5 m, which corresponded to the pulsating section of the model. It can be concluded that the enlargement of the surface area of the folds with a decrease in inlet velocity and pressure along the intestinal model enhanced nutrient delivery to the internal wall. Fluid (food supplements) physical properties can significantly affect the relaxation and contraction of the movement (peristalsis) along the gastrointestinal tract and, by extension, impact the healthy living. Ogi required more pressure for effective flow at all inlet velocities due to its highest viscosity. To ensure effective flow and circumvent complications when taking food supplements, especially for someone under medication, a flow velocity of 0.005 m/s is recommended. The presence of villi in the intestinal wall improves nutrient absorption and augments heat transfer.

Nomenclature

ρ	Fluid density
m	Mass of fluid
v	Volume of the fluid
d	Sphere falling distance
t	Time
μ	Dynamic fluid viscosity
r_s	Radius of the sphere
ρ_s	Density of the sphere
v_s	Velocity of the sphere
ρ_l	Density of the prepared samples
g	Acceleration due to gravity
$\bar{Z}$	Axis lies along the centerline of the tube
$\bar{R}$	Coordinate transverse to the center line
μ_O	Zero shear rate viscosity
Γ	Characteristic time
Π	Second invariant strain tensor
V	Velocity vector
P	Pressure
k	Thermal conductivity
T	Fluid temperature
C_p	Specific heat capacity
$\bar{W}$	Velocity components in the axial direction
$\bar{U}$	Velocity components in the radial direction
$\bar{\tau}$	Extra shear stress tensor
$\bar{\dot{\gamma}}$	Shear rate
μ_∞	Infinite shear rate viscosity

References

1. Adegun, I.K., Ibrahim, I.B., and Adesoye, O.A. "Numerical simulation of laminar flow of non-Newtonian

fluids in a rhythmical non-permeable medium", *An NNALS Fac. Eng. Hunedoara–Int. J. Eng.*, **Tome XVII**, pp. 175–180 (Feb. 1, 2019).

2. Burclaff, J., Bliton, R.J., Breau, K.A., et al. "A proximal-to-distal survey of healthy adult human small intestine and colon epithelium by single-cell transcriptomics", *Cmgh.*, **13**(5), pp. 1554–1589 (2022). DOI: 10.1016/j.jcmgh.2022.02.007

3. Farooq, S., IjazKhan, M., Hayat, T., et al. "Theoretical investigation of peristalsis transport in the flow of hyperbolic tangent fluid with slip effects and chemical reaction", *J. Mol. Liq.*, **285**, pp. 314–322 (2019). DOI: 10.1016/j.molliq.2019.04.051

4. Adegun, I.K., Ibitoye, S.E., and Bala, A. "Effect of selected geometric parameters on natural convection in concentric square annulus", *Aust. J. Mech. Eng.*, **20**(4), pp. 1–12 (2020). DOI: 10.1080/14484846.2020.1784559

5. Akram, J., Akbar, N.S., and Tripathi, D. "Electroosmosis augmented MHD peristaltic transport of SWCNTs suspension in aqueous media", *J. Therm. Anal. Calorim.*, **147**(3), pp. 2509–2526 (2022). DOI: 10.1007/s10973-021-10562-3

6. Norton, T. and Sun, D.W. "Computational fluid dynamics (CFD) - an effective and efficient design and analysis tool for the food industry: A review", *Trends Food Sci. Technol.*, **17**(11), pp. 600–620 (2006). DOI: 10.1016/j.tifs.2006.05.004

7. Lege, A.J. "Mathematical and numerical modelling of peristaltic flow and absorption in the small intestine", PhD Thesis, Bath Univ. (2014).

8. Tripathi, D., Prakash, J., Gnaneswara Reddy, M., et al. "Numerical study of electroosmosis-induced alterations in peristaltic pumping of couple stress hybrid nanofluids through microchannel", *Indian J. Phys.*, **95**, pp. 2411–2421 (2020). https://doi.org/10.1007/s12648-020-01906-0

9. Wright, J., Wulfert, F., Hort, J., et al. "Effect of preparation conditions on release of selected volatiles in tea headspace", *J. Agric. Food Chem.*, **55**, pp. 1445–1453 (2017).

10. Alokaily, S. "Modeling and simulation of the peristaltic flow of Newtonian and non-Newtonian fluids with application to the human body", PhD Thesis: Department of Mathematical Sciences Michigan Technological University (2017).

11. Olayemi, O.A., Al-Farhany, K., Ibitoye, S.E., et al. "Mixed convective heat transfer in a lid-driven concentric trapezoidal enclosure: numerical simulation", *International Journal of Engineering Research in Africa*, **60**, pp. 43–62 (2022). https://doi.org/10.4028/p-kybe41

12. Arian, C.M., Imaoka, T., Yang, J., et al. "Gutsy science: In vitro systems of the human intestine to model oral drug disposition", *Pharmacol. Ther.*, **230**, 107962 (2022). DOI: 10.1016/j.pharmthera.2021.107962

13. Hashimoto, Y., Michiba, K., Maeda, K., et al. "Quantitative prediction of pharmacokinetic properties of drugs in humans: Recent advance in vitro models to predict the impact of efflux transporters in the small intestine and blood-brain barrier", *J. Pharmacol. Sci.*, **148**(1), pp. 142–151 (2022). DOI: 10.1016/j.jphs.2021.10.010

14. Karthikeyan, J.S., Salvi, D., and Karwe, M.V. "Modeling of fluid flow, carbohydrate digestion, and glucose absorption in human small intestine", *J. Food Eng.*, **292**, p. 110339 (2021). DOI: 10.1016/j.jfoodeng.2020.110339

15. kram, J., Sher, N., and Tripathi, D. "Analysis of electroosmotic flow of silver-water nanofluid regulated by peristalsis using two different approaches for nanofluid", *J. Comput. Sci.*, **62**, p. 101696 (2022). DOI: 10.1016/j.jocs.2022.101696

16. Arrieta, J., Cartwright, J.H.E., Gouillart, E., et al. "Geometric mixing, peristalsis, and the geometric phase of the stomach", **10**(7), pp. 1–17 (2015). DOI: 10.1371/journal.pone.0130735

17. Ehsan, T., Anjum, H.J., and Asghar, S. "Peristaltic flows: A quantitative measure for the size of a bolus", *Physica A: Statistical Mechanics and its Applications*, **553**(C), 124211 (2020). DOI: 10.1016/j.physa.2020.124211

18. Chen, Y., Zhou, W., Roh, T. et al. "In vitro enteroid-derived three-dimensional tissue model of human small intestinal epithelium with innate immune responses", *PLoS One*, **12**(11), pp. 1–20 (2017).

19. Cortez, A.R., Poling, H.M., Brown, N.E., et al. "Transplantation of human intestinal organoids into the mouse mesentery: A more physiologic and anatomic engraftment site", *Surgery*, **164**(4), pp. 643–650 (2018). DOI: 10.1016/j.surg.2018.04.048

20. Imam, H., Sanmiguel, C., Larive, B., et al. "Study of intestinal flow by combined videofluoroscopy", *Am. J. Physiol. Liver Physiol.*, **286**, pp. 263–270 (2018).

21. Ellahi, R., Bhatti, M.M., and Vafai, K. "International journal of heat and mass transfer effects of heat and mass transfer on peristaltic flow in a non-uniform rectangular duct", *Int. J. Heat Mass Transf.*, **71**, pp. 706–719 (2014). DOI: 10.1016/j.ijheatmasstransfer.2013.12.038

22. Farooq, S., Hayat, T., Alsaedi, A., et al. "Mixed convection peristalsis of corban nanotubes with thermal radiation and entropy generation", *J. Mol. Liq.*, **250**, pp. 451–467 (Jan. 2018). DOI: 10.1016/j.molliq.2017.11.179

23. Nadeem, S., Ashiq, S., and Ali, M. "Williamson fluid model for the peristaltic flow of chyme in small intestine", *Mathematical Problems in Engineering*, **2012**, pp. 1–18 (2012). DOI: 10.1155/2012/479087

24. Mernone, A.V. "A mathematical study of peristaltic transport of physiological fluids“, PhD Thesis, Department of Applied Mathematics, Adelaide University (2000).

25. Levy, I., Reifen, R., Livny, O., et al. "Bcarotene bioavailability from differently processed carrot meals in human ileostomy volunteers", *Eur. J. Nutr.*, **42**, pp. 338–345 (2016).

26. Tripathi, D., Akbar, N.S., and Khan, Z.H. "Peristaltic transport of bi-viscosity fluids through a curved tube: A mathematical model for intestinal flow", *J. Eng. Med.*, **230**(9), pp. 817–828 (2016). DOI: 10.1177/0954411916658318

27. Javed, M. and Naz, R. "Peristaltic flow of a realistic fluid in a compliant channel", *Physica A*, p. 123895 (2020). DOI: 10.1016/j.physa.2019.123895

28. Rabe, S., Linforth, R.S.T., Krings, U., et al. "Volatile release from liquids. A comparison of in vivo Apci-Ms, in-mouth headspace trapping and in vitro mouth model data", *Chem. Senses Flavor*, **29**, pp. 163–173 (2014).

29. Schulte, L., Hohwieler, M., Müller, M., et al. "Intestinal organoids as a novel complementary model to dissect inflammatory bowel disease", *Stem Cells International*, **2019**, pp. 1–15 (2019). https://doi.org/10.1155/2019/8010645

30. Kamaltdinov, M., Trusov, P., and Zaitseva, N. "A multiphase flow in the an troduodenum: some results of the mathematical modeling and computational simulation", *MATEC Web of Conferences*, **145**, p. 04002 (2018).
https://doi.org/10.1051/matecconf/201814504002

31. Rosalia, M. and Fonseca, J. "An engineering understanding of the small intestine", PhD Thesis Sch. Chem. Eng. Univ. Birmingham (2011).

32. Tharakan, A., Rayment, P., Fryer, P.J., et al. "Modelling of physical and chemical processes in the small intestine", PhD Thesis Cent. Formul. Eng. Dep. Chem. Eng. Univ. Birmingham, no. September, pp. 1–302 (2008).

33. Abbas, N., Nadeem, S., Saleem, A., et al. "Analysis of non-Newtonian fluid with phase flow model", *Sci. Iran.*, **28**(6F), pp. 3743–3752 (2021). DOI: 10.24200/sci.2021.53475.3258

34. Tripathi, D. and Bég, O.A. "Mathematical biosciences peristaltic propulsion of generalized Burgers' fluids through a non-uniform porous medium: A study of chyme dynamics through the diseased intestine", *Math. Biosci.*, **248**, pp. 1–11 (2013). DOI: 10.1016/j.mbs.2013.11.006

35. Marciani, L., Gowland, P.A., Spiller, R.C., et al. "Effect of meal viscosity and nutrients on satiety, intragastric dilution, and emptying", *Am. J. Physiol Gastrointest Liver Physiol*, **280**, pp. 227–33 (2015).

36. Maxime, M.M., Brown, N.E., Poling, H.M., et al. "In vivo model of small intestine", **1597**, pp. 229–245 (2017). DOI: 10.1007/978-1-4939-6949-4

37. Marrero, D., Pujol-Vila, F., Vera, D., et al. "Gut-on-a-chip: Mimicking and monitoring the human intestine", *Biosens. Bioelectron.*, **181**, p. 113156 (2021). DOI: 10.1016/j.bios.2021.113156

38. Ashraf, R., Suhail, A., Mustafa, A.U., et al. "Measuring viscosity of different fluids using ball drop method", *ASME, MEL III*, pp. 1–5 (2018).

39. Yusuf, T.A., Bolaji, B.O., Ismaila, S.O., et al. "Determination of thermo physical properties of Water-Extract from Fermented Ground Maize (WEFGM) as possible alternative to water use as cutting fluid", *Silpakorn Univ. Sci. Technol. J.*, **10**(2), pp. 51–60 (2016).

40. Nadeem, S., Amin, A., Abbas, N., et al. "Effects of heat and mass transfer on stagnation point flow of micropolar Maxwell fluid over Riga plate", *Sci. Iran.*, **28**(6 F), pp. 3753–3766 (2022). DOI: 10.24200/sci.2021.53858.3454

41. Ibitoye, S.E., Adegun, I.K., Omoniyi, P.O., et al. "Numerical investigation of thermo-physical properties of the non-Newtonian fluid in a modeled intestine", *J. Bioresour. Bioprod.*, **5**(3), pp. 211–221 (2020). DOI: 10.1016/j.jobab.2020.07.007

42. Van de Wiele, T., Van den Abbeele, P., Ossieur, W., et al., *The Simulator of the Human Intestinal Microbial Ecosystem*, Cham (CH): Springer (2015). DOI: 10.1007/978-3-319-16104-4_27

43. Stoll, B.R., Batycky, R.P., Leipold, H.R., et al. "A theory of molecular absorption from the small intestine", *Chem. Eng. Sci.*, **55**, pp. 473–489 (2016).

44. Ismail, A.A. "Peristaltic flow of some selected food supplements in a modeled esophagus", M. Eng. Thesis Dep. Mech. Eng., Fac. Eng. Univ. Ilorin, pp. 1–150 (2017).

Biographies

Segun Emmanuel Ibitoye is a Lecturer at the Department of Mechanical Engineering, University of Ilorin, Nigeria. He is a registered professional engineer at the Council for the Regulation of Engineering in Nigeria (COREN). His research interests include renewable energy (biomass), materials characterization, numerical modeling, simulation, and mechanical engineering design.

Isaac Kayode Adegun is a Mechanical Engineering Professor and a Lecturer at the Department of Mechanical Engineering, University of Ilorin, Nigeria. He has supervised several master and PhD students. He is a registered professional engineer at the Council for the Regulation of Engineering in Nigeria (COREN). His research interests are heat transfer, numerical modeling, and simulation.

Olalekan Adebayo Olayemi is currently a PhD Researcher at the School of Aerospace, Transportation and Manufacturing, Cranfield University, United

Kingdom and a lecturer at the Department of Aeronautical and Astronautical Engineering, Kwara State University, Malete, Kwara State, Nigeria. His research interests involve thermofluids, computational fluid dynamics, and aerodynamics. He has published works in peer-reviewed journals in his areas of interest. He is a member of the Nigerian Society of Engineers (MNSE) and a registered Professional Engineer at the Council for the Regulation of Engineering in Nigeria (COREN).

Peter Olorunleke Omoniyi is currently a Lecturer at the Department of Mechanical Engineering, University of Ilorin, Nigeria. He is a registered professional engineer at the Council for the Regulation of Engineering in Nigeria (COREN). His major research focus is on different aspects of simulation, welding, and additive manufacturing.

Oluwaseyi Omotayo Alabi completed his MSc degree at the Department of Mechanical Engineering, University of Ilorin, Nigeria. His major research focus is on different aspects of heat transfer, modeling, and simulation.